

Precision lattice QCD computation of the $B^*B\pi$ coupling

ALPHA Collaboration

Fabio Bernardoni^a, John Bulava^{b,*}, Michael Donnellan^a, Rainer Sommer^a^a NIC @ DESY, Platanenallee 6, 15738 Zeuthen, Germany^b School of Mathematics, Trinity College, Dublin 2, Ireland

ARTICLE INFO

Article history:

Received 16 September 2014

Received in revised form 22 November 2014

Accepted 25 November 2014

Available online 2 December 2014

Editor: B. Grinstein

Keywords:

Lattice QCD

Heavy quark effective theory

Bottom quarks

Heavy meson chiral effective theory

ABSTRACT

The static $B^*B\pi$ coupling, \hat{g}_χ , a low energy constant in the leading order heavy meson chiral Lagrangian, is determined using $N_f = 2$ lattice QCD. We use CLS ensembles with lattice spacings and pion masses down to $a = 0.05$ fm and $m_\pi = 270$ MeV, and perform combined continuum and chiral extrapolations of our results which have a much better accuracy than previous numbers in the literature. As a by-product, we determine the coupling between the first radial excitations in the B and B^* channels (\hat{g}_{22}). Accounting for all uncertainties, which are dominated by the chiral extrapolation, we obtain $\hat{g}_\chi = 0.492(29)$, while \hat{g}_{22} is somewhat smaller. The comparison to a precise quenched computation suggests that there is little influence by the sea quarks and \hat{g}_χ will not change much when a dynamical strange quark is included.

© 2014 The Authors. Published by Elsevier B.V. This is an open access article under the CC BY license (<http://creativecommons.org/licenses/by/3.0/>). Funded by SCOAP³.

1. Introduction

Low energy QCD is described by an effective theory based on spontaneously broken global $SU(N_f)_L \times SU(N_f)_R$ chiral symmetry, where N_f is the number of light quark flavors. At the same time, a low energy expansion of hadrons with a single heavy quark with mass m_h exists and is known as heavy quark effective theory [1–4]. These chiral and heavy quark expansions may be combined to construct effective theories for the low-energy dynamics of hadrons containing a single heavy quark [5–7].

The theory that describes mesons is called Heavy Meson Chiral Perturbation Theory (HM χ PT) and contains a single additional leading low energy constant with respect to standard χ PT. This additional low energy constant, \hat{g}_χ , describes the coupling of heavy mesons to pseudo-Goldstone bosons in the chiral ($m_\pi^2 \rightarrow 0$) and static ($m_h \rightarrow \infty$) limits.

The coupling \hat{g}_χ is relevant for the computation of B-physics matrix elements from lattice QCD, exemplified by the ALPHA Collaboration HQET program [8–12]; it enters in chiral extrapolations of hadronic parameters needed for heavy flavor phenomenology, such as the B-meson decay constant and the B-meson semileptonic decay form factors. This coupling is also referred to as

the $B^*B\pi$ coupling, where the pseudoscalar and vector static-light mesons are denoted B and B^* . Note that the static ($m_h \rightarrow \infty$) limit is implied.

One way to determine \hat{g}_χ is through phenomenological fits to experimental data. A determination from $D^* \rightarrow D\pi$ decays [13] yields a value of $\hat{g} = 0.61(6)$. However, this extraction is affected by $O(1/m_c)$ and $O(m_\pi^2)$ errors, where especially the first ones are hard to estimate. Unfortunately, the process $B^* \rightarrow B\pi$ is kinematically forbidden, complicating the estimation of the $O(1/m_h)$ errors from experimental results. For a recent review of results, including also quark model and QCD sum rules calculations, see Ref. [14].

In this work we employ a different approach. Using lattice QCD simulations, we calculate a matrix element of the (light–light) axial current in QCD which is equivalent to \hat{g}_χ in leading order HM χ PT. Namely, we compute (ignoring renormalization and improvement in this introduction)

$$\hat{g} = \frac{1}{2} \langle B^0(\mathbf{0}) | \hat{A}_k(0) | B_k^{*+}(\mathbf{0}) \rangle, \quad \hat{A}_\mu(x) = \bar{\psi}_d(x) \gamma_\mu \gamma_5 \psi_u(x), \quad (1.1)$$

where ψ_d (ψ_u) annihilates a down (up) quark and the index $k = 1, 2, 3$ is not summed over. We use the finite volume normalization of states $\langle B^0(\mathbf{p}) | B^0(\mathbf{p}) \rangle = \langle B^*(\mathbf{p}) | B^*(\mathbf{p}) \rangle = 2L^3 = 2V$, where L is the linear size of the simulated torus. We work directly in the static limit for the heavy quark, but at finite light quark mass.

* Corresponding author.

E-mail address: jbulava@maths.tcd.ie (J. Bulava).

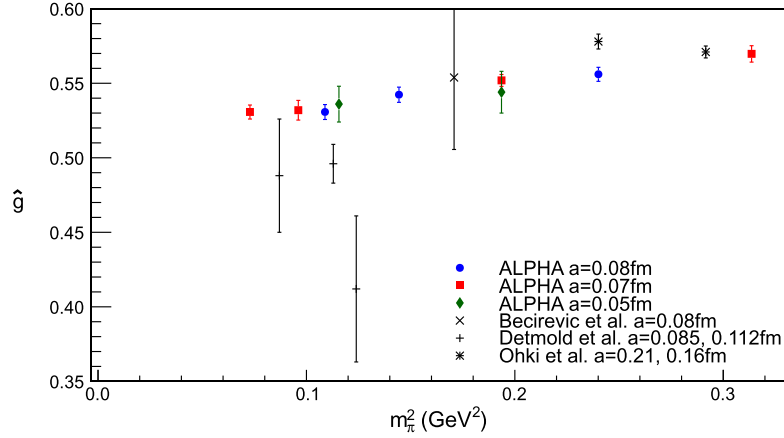


Fig. 1. A summary of unquenched lattice QCD results for \hat{g} . The results from the three lattice spacings used in this work are labeled 'ALPHA'. Additionally there are results of Ohki et al. [16], Becirevic et al. [17] and Detmold et al. [18]. For Ref. [18], which employs $N_f = 2 + 1$ dynamical flavors, we take the results for a single level of link smearing in the static action.

Therefore \hat{g}_χ is eventually obtained by an extrapolation of our results for \hat{g} to the zero light quark mass (chiral) limit as well as the $a \rightarrow 0$ (continuum) limit, where a is the lattice spacing of our simulations.

There have been previous determinations of \hat{g}_χ using lattice QCD with $N_f = 0, 2, 3$ dynamical light quark flavors directly in the static limit [15–18], as well as determinations at the charm [19] and bottom [20] points. However, the lattice spacing dependence of this quantity has not yet been thoroughly investigated. In this work we perform a continuum extrapolation in both the $N_f = 0$ and $N_f = 2$ theories and find small lattice spacing effects for our $O(a)$ improved discretization.

In Fig. 1 we compare our results (before extrapolations) to recent lattice results from Refs. [16–18]. We observe that a new quality is reached, reducing previous uncertainties by an order of magnitude in the region of interest, namely at small pion masses.¹ This is achieved by both improved techniques [21] and good statistics.

Additionally, we quote results for the matrix element of the first radial excitations. To this end we define

$$\hat{g}_{mn}(y, a) = \frac{1}{2} \langle B^0(\mathbf{0}), m | \hat{A}_k(0) | B_k^{*+}(\mathbf{0}), n \rangle \quad (1.2)$$

where $m, n = 1$ are the ground states of B and B^* mesons while $m, n > 1$ refer to their excitations. Apart from our main object of study, $\hat{g}_{11} = \hat{g}$, we quote rough numbers for \hat{g}_{22} . Preliminary results for \hat{g}_{11} and \hat{g}_{22} have appeared in Ref. [22] (together with results for \hat{g}_{12}) and a preliminary account of our present work can be found in Ref. [23]. The variable y is proportional to the square of the pion mass and will be defined when we discuss the chiral and continuum limit to arrive at $\hat{g}_\chi \equiv \hat{g}_{11}(0, 0)$ and $\hat{g}_{22}^\chi \equiv \hat{g}_{22}(0, 0)$.

In Section 2 we describe our techniques. In Section 3.1 we show results in the quenched approximation, where a continuum limit is taken for both \hat{g}_{11} and \hat{g}_{22} at a fixed quark mass $m_q \approx m_{\text{strange}}$. In Section 3.2 we discuss the $N_f = 2$ results, in particular the chiral and continuum extrapolations. Finally we conclude in Section 4.

2. Methodology

Here we describe some details of the lattice calculation of \hat{g}_{mn} , namely the proper definition of the axial current and the

technology to obtain precise matrix elements from correlation functions including the estimation of systematic errors due to excited state contributions. We also detail our stochastic technique utilizing translation invariance. The ensembles used in the numerical application are explained in Sections 3.1 and 3.2.

2.1. Discretization and renormalization

We employ both the HYP1 and HYP2 discretizations of the static quark action [24,25] to mitigate the signal-to-noise problem and provide a further check on discretization effects. Generally, results from these two discretizations are compatible within statistical errors, but they are also strongly correlated. We will thus show both of them in the tables, but only use HYP2 in the detailed analysis.

The light quarks are non-perturbatively $O(a)$ improved Wilson quarks [26–28] and the improved and renormalized axial current is

$$(A_R)_k = Z_A(1 + b_A a m_q)(A_k + c_A \partial_k P), \quad (2.1)$$

where A_k has exactly the form given before and $P(x) = \bar{\psi}_d(x) \gamma_5 \times \psi_u(x)$ is the appropriate pseudoscalar density. For the required values of the bare coupling, the renormalization constant Z_A is known non-perturbatively for both $N_f = 0$ [29] and $N_f = 2$ [30,31] while for the improvement coefficient b_A we use the expansion in the bare coupling g_0^2 to first order with the one-loop coefficient of Ref. [32]. For our zero momentum transfer matrix element \hat{g} , the $\partial_k P$ term vanishes identically; c_A is not needed.

2.2. Matrix elements from the GEVP

The matrix elements \hat{g}_{mn} are accessible in lattice QCD via three-point correlation functions in Euclidean time, which (from the transfer matrix formalism) have the following representation

$$\begin{aligned} C_{ij}^{3\text{pt}}(t_1, t_2) &= a^3 \sum_{\mathbf{x}} \langle \mathcal{O}_i(t_1 + t_2) (A_R)_k(t_2, \mathbf{x}) \mathcal{O}_j^\dagger(0) \rangle \\ &= \sum_{m,n} \psi_{im} \psi_{jn}^* 2 \hat{g}_{mn} e^{-E_m t_1} e^{-E_n t_2}, \end{aligned} \quad (2.2)$$

where $\hat{\mathcal{O}}_i$ and $\hat{\mathcal{O}}_j^k$ are suitable interpolating fields for the B^0 and B_k^{*+} mesons (respectively), $\psi_{im} = \langle 0 | \hat{\mathcal{O}}_i | B, m \rangle = \langle 0 | \hat{\mathcal{O}}_i^k | B_k^*, m \rangle$ and E_m is the energy of the m th state. In the static limit the B and B^*

¹ We do not have access to the numerical results of Ref. [20] but their Fig. 2 shows errors similar to Refs. [17,18].

energy levels are the same and furthermore C_{ij}^{3pt} is independent of k as indicated by our notation.

To isolate the desired matrix elements, we also require the two-point correlation functions

$$C_{ij}^{2pt}(t) = \langle \mathcal{O}_i(t) \mathcal{O}_j^\dagger(0) \rangle = \sum_m \psi_{im} \psi_{jm}^* e^{-E_m t}. \quad (2.3)$$

Rather than analyzing $C^{3pt}(t_1, t_2)$ directly, we employ

$$D_{ij}^{3pt}(t) = \sum_{t_2=0}^{T-1} C_{ij}^{3pt}(t - t_2, t_2), \quad (2.4)$$

where the position of the current insertion is summed over [23,33,34]. The use of this summed correlation function improves the convergence in t but was proposed in Ref. [33] for different reasons.

In order to extract the desired matrix elements we choose a set of N interpolating operators and form the $N \times N$ correlation matrices $C_{ij}^{2pt}(t)$ and $D_{ij}^{3pt}(t)$. We then employ solutions of a generalized eigenvalue problem (GEVP) [35–37] to accelerate the asymptotic (in t) behavior and enable the extraction of \hat{g}_{nn} for $n > 1$.

It has been proven recently that the GEVP may be combined with summed insertions [21,22] to achieve a further reduction in the contribution from excited states. It was demonstrated that the summed insertion is particularly advantageous in the extraction of excited state matrix elements when compared to the ordinary GEVP. For completeness, we review the main points. We begin by solving the following GEVP

$$C^{2pt}(t) v_n(t, t_0) = \lambda_n(t, t_0) C^{2pt}(t_0) v_n(t, t_0), \quad (2.5)$$

where $t_0 \geq t/2$. It can be shown [21] that

$$\begin{aligned} M_n^{\text{eff}}(t, t_0) &= -\frac{1}{2} \partial_t \frac{(v_n(t, t_0), [D^{3pt}(t) \lambda_n^{-1}(t, t_0) - D^{3pt}(t_0)] v_n(t, t_0))}{(v_n(t, t_0), C^{2pt}(t) v_n(t, t_0))} \\ &= \hat{g}_{nn} + \mathcal{O}(e^{-\Delta_{N,n} t}), \end{aligned} \quad (2.6)$$

$$= \hat{g}_{nn} + \mathcal{O}(e^{-\Delta_{N,n} t}), \quad (2.7)$$

where $\Delta_{N,n} = E_{N+1} - E_n$ and (\cdot, \cdot) denotes an inner product over the GEVP indices. The important result is that (asymptotically) the corrections fall exponentially in $\Delta_{N,n} t$. The large energy gap $\Delta_{N,n}$, which in our application is above 1 GeV, is a virtue of the GEVP and the factor t is due to the summed insertion. Without summation, t would be replaced by $\min(t_1, t_2)$, see Eq. (2.2). We also note that the GEVP renders excited state matrix elements accessible.

In our numerical application, the interpolating fields $\mathcal{O}_i(x_0) = a^3 \sum_{\mathbf{x}} \bar{\psi}_b(\mathbf{x}) \Gamma_i \gamma_5 \psi_d(\mathbf{x})$ and $\mathcal{O}_i^k(x_0) = a^3 \sum_{\mathbf{x}} \bar{\psi}_u(\mathbf{x}) \Gamma_i \gamma_k \psi_b(\mathbf{x})$ are constructed from Gaussian smearing operators

$$\Gamma_i = (1 + \kappa_G a^2 \Delta)^{R_i}, \quad i = 1, 2, 3, \quad (2.8)$$

where Δ is the gauge-covariant spatial Laplace operator with APE-smeared links. The approximate width $r_i \approx 2a\sqrt{\kappa_G R_i}$ is chosen to keep the smearing radii at $r_i \approx 0.2, 0.3, 0.7$ fm for each lattice spacing. More details about the construction of these wavefunctions can be found in Refs. [8,10].

From the correlation functions we construct $M_n^{\text{eff}}(t) \equiv M_n^{\text{eff}}(t, t - a)$ and examine the large t behavior. Beginning with $t \approx r_0 \approx 0.5$ fm, we increase t until the asymptotic corrections due to excited states are small enough so that

$$|M_n^{\text{eff}}(t) - M_n^{\text{eff}}(t - \delta t)| < \sigma(t) \quad (2.9)$$

where $\delta t = \frac{1}{\Delta_{N,n}}$ and $\sigma(t)$ is the statistical (1σ) error on $M_n^{\text{eff}}(t)$. We call the first t at which this condition is satisfied t_{\min} . Under the assumption that the asymptotic decay Eq. (2.7) has roughly set in at t_{\min} , our requirement of Eq. (2.9) means that statistical errors exceed systematic ones by a factor $e - 1 \approx 2$ at $t = t_{\min}$. We then define our estimate of \hat{g}_{nn} as the weighted average of $M_n^{\text{eff}}(t)$ over the range $[t_{\min}, t_{\max}]$ with t_{\max} chosen to avoid points with excessive statistical errors. The estimate for the statistical error on $M_n^{\text{eff}}(t)$ will be discussed in future sections, in particular for the $N_f = 2$ results where autocorrelations must be treated with care.

2.3. Use of random sources

In order to reduce statistical fluctuations, we use full translation invariance everywhere. We achieve this by a stochastic estimation of one of the spatial sums, using [38] a random $U(1)$ source on each time-slice of the lattice ('time-dilution' [39]) and a 'sequential inversion' (Eq. (2.13) below) for the insertion of the axial current.

The explicit expression for the two-point function is

$$\begin{aligned} C_{ij}^{2pt}(y_0 - t_0) &= a^7 \sum_{\mathbf{y}, \mathbf{x}} \langle \eta_r^\dagger(\mathbf{x}; t_0) \Gamma_j \gamma_5 S_b(\mathbf{x}, \mathbf{y}) \Gamma_i \gamma_5 \Phi_r(\mathbf{y}; t_0) \rangle, \end{aligned} \quad (2.10)$$

$$[\mathcal{D} \Phi_r](\mathbf{y}; t_0) = \eta_r(\mathbf{y}; t_0), \quad (2.11)$$

where $\eta_r(\mathbf{y}; t_0) \propto \delta(y_0 - t_0) \in U(1)$ is a random $U(1)$ field on timeslice t_0 and vanishes otherwise, $S_b(\mathbf{x}, \mathbf{y})$ is the easily computed static quark propagator of the b-quark and \mathcal{D} is the Dirac operator of the light quarks. The subscript r enumerates the random source fields. Similarly, the three-point functions with summed current insertions read

$$\begin{aligned} D_{ij}^{3pt}(y_0 - t_0) &= Z_A(1 + b_A a m_q) a^7 \\ &\times \sum_{\mathbf{y}, \mathbf{x}} \langle \eta_r^\dagger(\mathbf{x}; t_0) \Gamma_j \gamma_k S_b(\mathbf{x}, \mathbf{y}) \Gamma_i \gamma_5 \tilde{\Phi}_{r,k}(\mathbf{y}; t_0) \rangle, \end{aligned} \quad (2.12)$$

$$[\mathcal{D} \tilde{\Phi}_{r,k}](\mathbf{y}; t_0) = \gamma_5 \gamma_k \Phi_r(\mathbf{y}; t_0). \quad (2.13)$$

In the numerical application, we average over $r = 1 \dots N_r$, all values $0 \leq t_0 \leq T - a$ and over $k = 1, 2, 3$. Hence, Eq. (2.11) and Eq. (2.13) add up to $N_r \times T/a \times 4$ Dirac equations which need to be solved on each gauge configuration. The ensemble average $\langle \cdot \rangle$ indicates an average over the random fields η_r as well as the gauge fields.

3. Results

We now discuss numerical results for $N_f = 0$ and $N_f = 2$. In both cases we employ the usual periodic and anti-periodic temporal boundary conditions for the gauge and fermion fields, respectively.

3.1. $N_f = 0$ continuum limit

We first apply the methods discussed in Section 2 to a set of three ensembles of quenched gauge configurations used previously in the ALPHA Collaboration HQET program [9], with the goal of taking the continuum limit of \hat{g}_{11} and \hat{g}_{22} . Details of the ensembles and measurements are given in Table 1. The valence quark mass on each of these ensembles was tuned to reproduce the physical strange quark mass [40].

The effective matrix elements $M_n^{\text{eff}}(t)$, $n = 1, 2$ for the $L/a = 16$ ensemble are shown together with their plateau averages in the left plot of Fig. 2. As autocorrelations play no role here, the errors

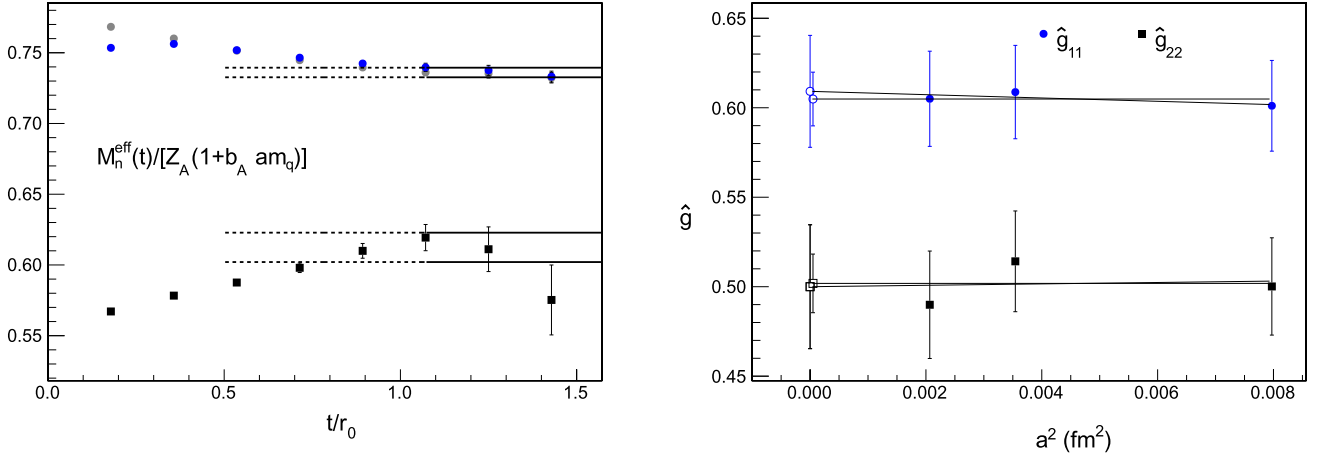


Fig. 2. Left: The bare effective matrix elements $M_n^{\text{eff}}(t)/[Z_A(1+b_A am_q)]$, $n = 1, 2$ for the HYP2 action together with the plateau averages denoted by solid lines. The gray points for $n = 1$ are the results obtained without the GEVP using the interpolator I_3 with smearing radius $r_3 \approx 0.7$ fm, while the dotted lines are simply meant to guide the eye. Right: The continuum limits for \hat{g}_{11} and \hat{g}_{22} for the HYP2 static quark action, taking $r_0 = 0.5$ fm.

Table 1

Details of the quenched ensembles used for the continuum extrapolations of \hat{g}_{11} and \hat{g}_{22} . The valence quark mass is chosen to be the strange quark mass [40] and the values for r_0/a are taken from Ref. [41].

β	κ	$(L^3/a) \times T/a$	r_0/a	N_{conf}	N_r
6.0219	0.133849	$16^3 \times 32$	5.6	100	200
6.2885	0.1349798	$24^3 \times 48$	8.4	100	48
6.4956	0.1350299	$32^3 \times 64$	11.0	100	32

are estimated using 100 single-elimination jackknife bins after first averaging over the N_r sources on each configuration. The range of the plateau averages is chosen according to the criteria in Section 2.

Finally, we perform continuum extrapolations of the renormalized axial current matrix elements. These extrapolations for \hat{g}_{11} and \hat{g}_{22} are shown in the right plot of Fig. 2 and suggest that cutoff effects are small for these quantities. Simple constant extrapolation of just the HYP2 action results yields $\hat{g}_{11}^{\text{strange}} = 0.605(15)$, $\hat{g}_{22}^{\text{strange}} = 0.502(16)$ while we take

$$\hat{g}_{11}^{\text{strange}} = 0.609(31), \quad \hat{g}_{22}^{\text{strange}} = 0.500(35) \quad \text{for } N_f = 0 \quad (3.1)$$

as our final quenched results, where a linear term in a^2 is allowed in the fit formula. It should be noted that our result for \hat{g}_{11} is compatible with the previous result of Ref. [23], but utilizes a more robust treatment of the systematic errors due to excited states, namely that of Section 2.

3.2. $N_f = 2$ results

We next use ensembles of the Coordinated Lattice Simulations (CLS) community effort. Details are tabulated in Table 2.

While we follow the same procedure to calculate the bare matrix elements, the large autocorrelations present in HMC simulations with periodic boundary conditions must be taken into account in order to safely estimate the statistical errors. To this end, we follow the procedure of Ref. [42] and attach an exponential ‘tail’ to the autocorrelation functions of the matrix elements, with a fall-off $\sim \exp(-t_{\text{MC}}/\tau_{\text{exp}})$, where τ_{exp} has been estimated roughly in Ref. [42].

A selection of the effective matrix elements is shown in Fig. 3. This figure also compares the use of the summed insertion with and without the GEVP for $M_1^{\text{eff}}(t)$. A clear picture for the difference is not easily seen for the few points available. However, the figure

Table 2

Details of the $N_f = 2$ ensembles. The pseudoscalar meson masses and lattice spacings are taken from Ref. [31] and N_r is as defined in Section 2. We also list our estimate of the exponential autocorrelation time τ_{exp} in units of the separation between configurations.

ID	β	m_π (MeV)	$(L_s^3 \times L_t)/a^4$	a (fm)	N_{conf}	τ_{exp}	N_r
A3	5.2	495	$32^3 \times 64$	0.076	1004	8	4
A4		385			1012	8	8
A5		332			500	6	4
E4	5.3	577	$32^3 \times 64$	0.066	157	17	48
E5		440			1000	8	4
F6		310	$48^3 \times 96$		500	17	4
F7		270			461	17	4
N5	5.5	440	$48^3 \times 96$	0.048	476	110	2
N6		340			400	25	2

indicates that while corrections are not necessarily smaller with the GEVP at small times $t \approx r_0/2$, the approach to the plateau is then accelerated soon after. Indeed, this is needed for our criteria Eq. (2.9) to apply.

For the excited state matrix element our statistical errors are not small enough to apply Eq. (2.9) to fix the start of the plateaux. Here we simply inspect the figures and choose a fixed $t_{\text{min}} \approx 0.5$ fm in physical units. The large statistical errors seem to dominate over the systematic errors due to excited state contributions. The renormalized matrix elements together with the statistical errors estimated using the additional exponential tail are collected in Table 3.

Next, the combined chiral and continuum extrapolation is performed. Let us first concentrate on the ground state matrix element, which yields \hat{g}_χ . We parametrize the quark mass dependence by the pion mass (as in Ref. [8]) through the variable² $y = m_\pi^2/(8\pi^2 f_\pi^2)$.

As already evident from Fig. 1, the data is rather linear in m_π^2 (or y), while chiral perturbation theory predicts a significant logarithmic modification [18,43]. We therefore perform two extrapolations to the chiral limit. Namely we fit to the two forms

$$\hat{g}_{11}^{\text{lin}}(y, a) = \hat{g}_\chi + By + Ca^2, \quad (3.2)$$

$$\hat{g}_{11}^{\text{NLO}}(y, a) = \hat{g}_\chi [1 - (1 + 2(\hat{g}_\chi)^2)y \log y] + By + Ca^2, \quad (3.3)$$

² Our normalization of the pion decay constant is such that it is $f_\pi \simeq 130$ MeV in the chiral limit.

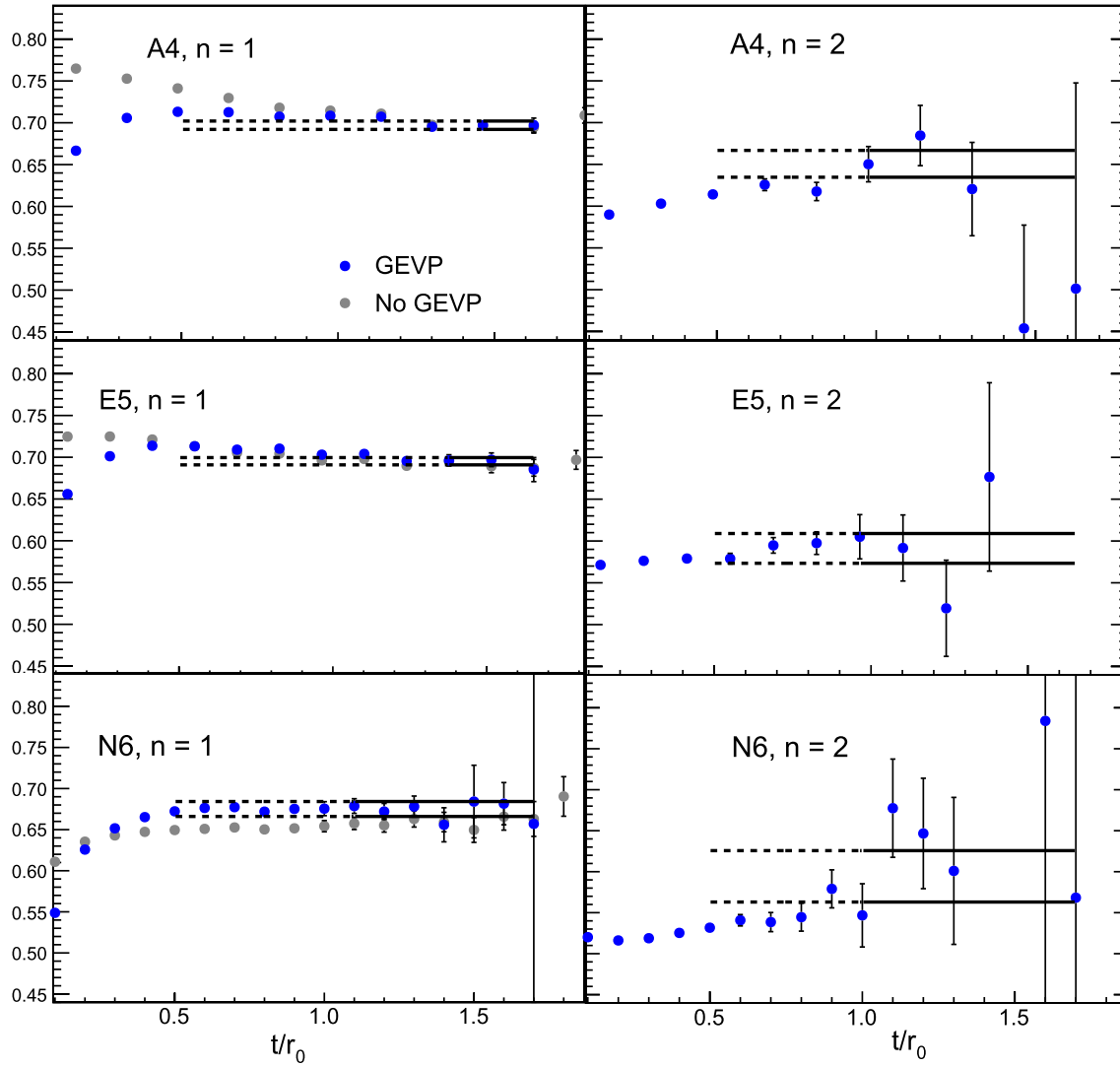


Fig. 3. The bare effective matrix elements for a selection of the $N_f = 2$ ensembles. The left column is $M_1^{\text{eff}}(t)$ while the right is $M_2^{\text{eff}}(t)$. The left column also shows the effective matrix elements obtained without the GEVP represented by the gray points as in Fig. 2. The solid lines show the plateau averages while the dotted lines are meant to guide the eye.

Table 3

$N_f = 2$ renormalized values for \hat{g}_{11} and \hat{g}_{22} for both HYP1 and HYP2 static quark actions. The errors are the combined statistical errors from the bare matrix elements (taking autocorrelations into account) and the renormalization constants. Note that no data for the HYP1 action is present for the N6 ensemble.

Ens. ID	$\hat{g}_{11}^{\text{HYP1}}$	$\hat{g}_{11}^{\text{HYP2}}$	$\hat{g}_{22}^{\text{HYP1}}$	$\hat{g}_{22}^{\text{HYP2}}$
A3	0.553(5)	0.556(5)	0.497(15)	0.505(14)
A4	0.537(6)	0.542(5)	0.498(14)	0.503(15)
A5d	0.528(5)	0.531(5)	0.516(18)	0.527(19)
E4	0.567(5)	0.570(6)	0.489(13)	0.494(14)
E5g	0.543(5)	0.546(5)	0.460(17)	0.464(17)
F6	0.531(7)	0.532(7)	0.470(17)	0.469(16)
F7	0.528(4)	0.531(5)	0.479(13)	0.477(13)
N5	0.541(15)	0.544(14)	0.477(72)	0.477(71)
N6	–	0.536(12)	–	0.465(43)

where B , C , and the desired \hat{g}_χ are fit parameters. In both forms, the Ca^2 term can probe cutoff effects and we consider terms of order ya^2 as too small to be relevant, as we do with a^3 and y^2 . In both fits, the results for C are compatible with zero. As our central values we take the fit results for \hat{g}_χ with C set to zero. The linear fit, Eq. (3.2), then yields $\hat{g}_\chi = 0.513(8)$ while the correct *asymptotic*

form, Eq. (3.3), extrapolates further down to $\hat{g}_\chi = 0.469(7)$. We combine these numbers to our central result

$$\hat{g}_\chi = 0.492(29). \quad (3.4)$$

The error is by far dominated by the difference of the two chiral extrapolations. We have chosen a range which encompasses the linear and the NLO extrapolation *and* their errors. Allowing for non-vanishing C changes rather little concerning this result.

Of course the situation is far from perfect: the theoretically well motivated functional form is not verified by the data; a linear dependence fits somewhat better. However, in the end we are interested in the extrapolated value and it seems very safe to assume that it lies in the range Eq. (3.4). Indeed, if NLO chiral behavior sets in at masses which are below the ones in Fig. 4, the downward bend will happen later and the result will be in between the two values shown in the figure and used to form Eq. (3.4).

For \hat{g}_{22} the functional form including chiral log's is not known. Also the data are much less precise. We thus perform a simple linear extrapolation both with and without an a^2 term. They are shown on the right side of Fig. 4. A range covering both results is

$$\hat{g}_{22} = 0.425(70). \quad (3.5)$$

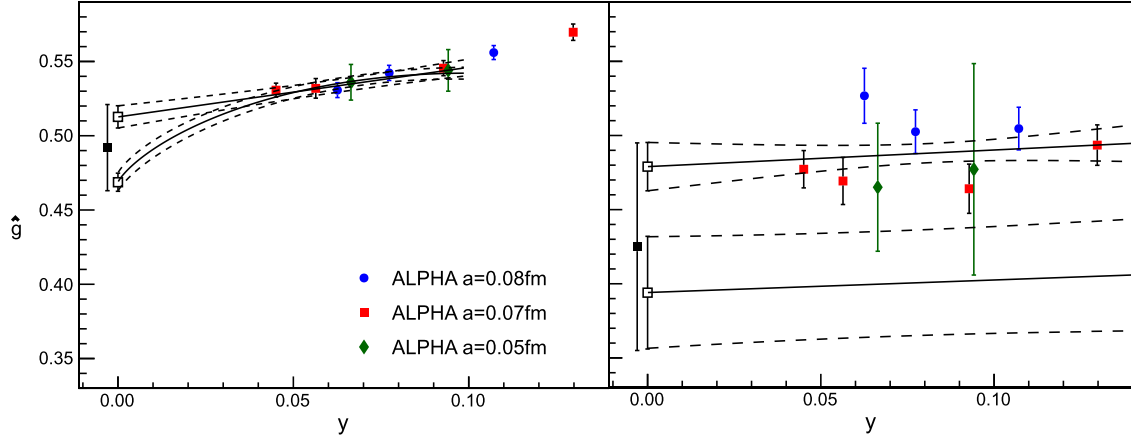


Fig. 4. A summary of \hat{g}_{11} (left) and \hat{g}_{22} (right) together with the extrapolated values and final results explained in the text. For \hat{g}_{11} , both linear and NLO chiral extrapolations are shown, while for \hat{g}_{22} we only perform a linear extrapolation. In the case of the excited state matrix element both the extrapolation with C as fit parameter (lower curve) and the one with $C = 0$ are shown.

4. Conclusions

In this paper we have presented a precise $N_f = 2$ determination of \hat{g}_χ , the leading low energy constant appearing in $\text{HM}\chi\text{PT}$ parametrizing the coupling of heavy-light mesons to pions. We have calculated the bare matrix elements using solutions of the GEVP together with the summed insertion technique, resulting in a precision which exceeds previous ones by an order of magnitude. We renormalized these matrix elements non-perturbatively.

We have taken the continuum and chiral limits assuming both a phenomenological linear behavior in the square of the pion mass and next-to-leading-order continuum $\text{HM}\chi\text{PT}$. Two discretizations of the static quark action serve as a further check on lattice spacing effects. These two discretizations give statistically compatible results for all quantities. Our central result is Eq. (3.4). This value, $\hat{g}_\chi = 0.49(3)$, improves in accuracy compared to previous estimates: $\hat{g}_\chi^{\text{quenched}} = 0.42(4)(8)$ [15], $\hat{g}_\chi = 0.52(1)(3)(3)$ [16], $\hat{g}_\chi = 0.44(3)(7)$ [17], $\hat{g}_\chi = 0.45(5)(2)$ [18], $\hat{g}_\chi^{\text{charm}} = 0.53(3)(3)$ [19] and $\hat{g}_\chi^{\text{bottom}} = 0.57(5)(6)$ [20]. Within the cited overall uncertainties all previous numbers are in agreement with our more precise value. In fact the agreement is better than one might have expected given that some numbers come from extrapolations from rather large pion masses and lattice spacings.

As discussed in Section 2, we have treated the systematic errors due to excited states in a conservative manner. Similarly, we have also safely estimated the statistical errors by including tails in the autocorrelation functions. At our finest lattice spacing, these are significant, see Section 3.2. However, in the end, the dominating uncertainty comes from the fact that the data does not appear to be at such small pion masses where NLO chiral behavior can be seen. Instead an approximately linear behavior in m_π^2 prevails down to $m_\pi = 270$ MeV. We thus take a final range which also covers the result of a simple linear extrapolation.

In comparison to the quenched result, we have to take into account that Eq. (3.1) is for a light quark mass set to the strange mass. This corresponds to $y \approx 0.2$, outside the range of Fig. 4. The figure then suggests that $N_f = 2$ and the quenched number agree within at least 5% precision. We do not see any sea quark effects at the strange mass. It thus appears safe to use Eq. (3.4) with its more than 5% error also for the three (or more) flavor theory.

Despite our limited control over the chiral limit, our determination of \hat{g}_χ is precise enough to help the chiral extrapolation of many quantities of phenomenological interest in heavy meson physics. It is therefore used broadly in the ALPHA Collaboration HQET program. This result may also be used (together with the

B and B^* decay constants) to constrain the large- q^2 behavior of the B meson semileptonic decay form-factor $f_+(q^2)$ [44] as well as in pole model parametrizations of $f_+(q^2)$ (see for example Ref. [45] and the references contained therein).

Acknowledgements

We thank Hubert Simma, David Lin, and Gilberto Colangelo for useful discussions, Benoit Blossier and Antoine Gérardin for providing us with data on the N6 ensemble from Ref. [22], and Patrick Fritzsche for useful comments on an earlier version of this manuscript. This work is supported by the Deutsche Forschungsgemeinschaft in the SFB/TR 09 and by the European community through EU Contract No. MRTN-CT-2006-035482, “FLAVIANet”. We are grateful to NIC and to the Norddeutsche Rechnerverbund for allocating computing resources to this project. Some of the correlation function measurements were performed on the PAX cluster at DESY, Zeuthen.

References

- [1] E. Eichten, B. Hill, An effective field theory for the calculation of matrix elements involving heavy quarks, *Phys. Lett. B* 234 (1990) 511.
- [2] N. Isgur, M.B. Wise, Weak decays in the static quark approximation, *Phys. Lett. B* 232 (1989) 113–117.
- [3] H. Georgi, An effective field theory for heavy quarks at low energies, *Phys. Lett. B* 240 (1990) 447–450.
- [4] E. Eichten, B. Hill, Static effective field theory: $1/m$ corrections, *Phys. Lett. B* 243 (1990) 427–431.
- [5] G. Burdman, J.F. Donoghue, Union of chiral and heavy quark symmetries, *Phys. Lett. B* 280 (1992) 287–291.
- [6] T.-M. Yan, H.-Y. Cheng, C.-Y. Cheung, G.-L. Lin, Y. Lin, et al., Heavy quark symmetry and chiral dynamics, *Phys. Rev. D* 46 (1992) 1148–1164.
- [7] M.B. Wise, Chiral perturbation theory for hadrons containing a heavy quark, *Phys. Rev. D* 45 (1992) 2188–2191.
- [8] F. Bernardoni, B. Blossier, J. Bulava, M. Della Morte, P. Fritzsche, et al., The b-quark mass from non-perturbative $N_f = 2$ Heavy Quark Effective Theory at $O(1/m_h)$, *Phys. Lett. B* 730 (2014) 171–177, arXiv:1311.5498.
- [9] ALPHA Collaboration, B. Blossier, et al., HQET at order $1/m$: III. Decay constants in the quenched approximation, *J. High Energy Phys.* 1012 (2010) 039, arXiv:1006.5816.
- [10] ALPHA Collaboration, B. Blossier, et al., HQET at order $1/m$: II. Spectroscopy in the quenched approximation, *J. High Energy Phys.* 1005 (2010) 074, arXiv:1004.2661.
- [11] B. Blossier, M. Della Morte, N. Garron, R. Sommer, HQET at order $1/m$: I. Non-perturbative parameters in the quenched approximation, *J. High Energy Phys.* 1006 (2010) 002, arXiv:1001.4783.
- [12] F. Bernardoni, B. Blossier, J. Bulava, M. Della Morte, P. Fritzsche, et al., Decay constants of B-mesons from non-perturbative HQET with two light dynamical quarks, arXiv:1404.3590.

- [13] CLEO Collaboration, A. Anastassov, et al., First measurement of $\Gamma(D^{*+})$ and precision measurement of $m_{D^{*+}} - m_{D^0}$, Phys. Rev. D 65 (2002) 032003, arXiv:hep-ex/0108043.
- [14] B. El-Bennich, M.A. Ivanov, C.D. Roberts, Strong $D^* \rightarrow D\pi$ and $B^* \rightarrow B\pi$ couplings, Phys. Rev. C 83 (2011) 025205, arXiv:1012.5034.
- [15] UKQCD Collaboration, G.M. de Divitiis, et al., Towards a lattice determination of the $B^*B\pi$ coupling, J. High Energy Phys. 10 (1998) 010, arXiv:hep-lat/9807032.
- [16] H. Ohki, H. Matsufuru, T. Onogi, Determination of $B^*B\pi$ coupling in unquenched QCD, Phys. Rev. D 77 (2008) 094509, arXiv:0802.1563.
- [17] D. Becirevic, B. Blossier, E. Chang, B. Haas, $g_{B^*B\pi}$ -coupling in the static heavy quark limit, Phys. Lett. B 679 (2009) 231–236, arXiv:0905.3355.
- [18] W. Detmold, C.D. Lin, S. Meinel, Calculation of the heavy-hadron axial couplings g_1 , g_2 , and g_3 using lattice QCD, Phys. Rev. D 85 (2012) 114508, arXiv:1203.3378.
- [19] D. Becirevic, F. Sanfilippo, Theoretical estimate of the $D^* \rightarrow D\pi$ decay rate, Phys. Lett. B 721 (2013) 94–100, arXiv:1210.5410.
- [20] J. Flynn, P. Fritzsch, T. Kawanai, C. Lehner, C. Sachrajda, et al., The $B^*B\pi$ coupling with relativistic heavy quarks, arXiv:1311.2251.
- [21] J. Bulava, M. Donnellan, R. Sommer, On the computation of hadron-to-hadron transition matrix elements in lattice QCD, J. High Energy Phys. 1201 (2012) 140, arXiv:1108.3774.
- [22] B. Blossier, J. Bulava, M. Donnellan, A. Gérardin, On the $B^{*'} \rightarrow B$ transition, Phys. Rev. D 87 (2013) 094518, arXiv:1304.3363.
- [23] ALPHA Collaboration, J. Bulava, M. Donnellan, R. Sommer, The $B^*B\pi$ coupling in the static limit, PoS LATTICE2010 (2010) 303, arXiv:1011.4393.
- [24] A. Hasenfratz, F. Knechtli, Flavor symmetry and the static potential with hypercubic blocking, Phys. Rev. D 64 (2001) 034504, arXiv:hep-lat/0103029.
- [25] M. Della Morte, A. Shindler, R. Sommer, On lattice actions for static quarks, J. High Energy Phys. 0508 (2005) 051, arXiv:hep-lat/0506008.
- [26] M. Lüscher, S. Sint, R. Sommer, P. Weisz, Chiral symmetry and $O(a)$ improvement in lattice QCD, Nucl. Phys. B 478 (1996) 365–400, arXiv:hep-lat/9605038.
- [27] M. Lüscher, S. Sint, R. Sommer, P. Weisz, U. Wolff, Non-perturbative $O(a)$ improvement of lattice QCD, Nucl. Phys. B 491 (1997) 323–343, arXiv:hep-lat/9609035.
- [28] ALPHA Collaboration, K. Jansen, R. Sommer, $O(a)$ improvement of lattice QCD with two flavors of Wilson quarks, Nucl. Phys. B 530 (1998) 185–203, arXiv:hep-lat/9803017.
- [29] M. Lüscher, S. Sint, R. Sommer, H. Wittig, Nonperturbative determination of the axial current normalization constant in $O(a)$ improved lattice QCD, Nucl. Phys. B 491 (1997) 344–364, arXiv:hep-lat/9611015.
- [30] M. Della Morte, R. Sommer, S. Takeda, On cutoff effects in lattice QCD from short to long distances, Phys. Lett. B 672 (2009) 407–412, arXiv:0807.1120.
- [31] P. Fritzsch, F. Knechtli, B. Leder, M. Marinkovic, S. Schaefer, et al., The strange quark mass and Lambda parameter of two flavor QCD, Nucl. Phys. B 865 (2012) 397–429, arXiv:1205.5380.
- [32] S. Sint, P. Weisz, Further results on $O(a)$ improved lattice QCD to one loop order of perturbation theory, Nucl. Phys. B 502 (1997) 251–268, arXiv:hep-lat/9704001.
- [33] L. Maiani, G. Martinelli, M. Paciello, B. Taglienti, Scalar densities and baryon mass differences in lattice QCD with Wilson fermions, Nucl. Phys. B 293 (1987) 420.
- [34] S. Capitani, M. Della Morte, G. von Hippel, B. Jager, A. Jüttner, et al., The nucleon axial charge from lattice QCD with controlled errors, Phys. Rev. D 86 (2012) 074502, arXiv:1205.0180.
- [35] C. Michael, I. Teasdale, Extracting glueball masses from lattice QCD, Nucl. Phys. B 215 (1983) 433.
- [36] M. Lüscher, U. Wolff, How to calculate the elastic scattering matrix in two-dimensional quantum field theories by numerical simulation, Nucl. Phys. B 339 (1990) 222–252.
- [37] B. Blossier, M. Della Morte, G. von Hippel, T. Mendes, R. Sommer, On the generalized eigenvalue method for energies and matrix elements in lattice field theory, J. High Energy Phys. 04 (2009) 094, arXiv:0902.1265.
- [38] R. Sommer, Leptonic decays of B and D mesons, Nucl. Phys. Proc. Suppl. 42 (1995) 186–193, arXiv:hep-lat/9411024.
- [39] J. Foley, et al., Practical all-to-all propagators for lattice QCD, Comput. Phys. Commun. 172 (2005) 145–162, arXiv:hep-lat/0505023.
- [40] ALPHA Collaboration, J. Garden, J. Heitger, R. Sommer, H. Wittig, Precision computation of the strange quark's mass in quenched QCD, Nucl. Phys. B 571 (2000) 237–256, arXiv:hep-lat/9906013.
- [41] ALPHA Collaboration, M. Guagnelli, R. Sommer, H. Wittig, Precision computation of a low-energy reference scale in quenched lattice QCD, Nucl. Phys. B 535 (1998) 389–402, arXiv:hep-lat/9806005.
- [42] ALPHA Collaboration, S. Schaefer, R. Sommer, F. Virotta, Critical slowing down and error analysis in lattice QCD simulations, Nucl. Phys. B 845 (2011) 93–119, arXiv:1009.5228.
- [43] W. Detmold, C.-J.D. Lin, S. Meinel, Axial couplings in heavy hadron chiral perturbation theory at the next-to-leading order, Phys. Rev. D 84 (2011) 094502, arXiv:1108.5594.
- [44] C.G. Boyd, B. Grinstein, Chiral and heavy quark symmetry violation in B decays, Nucl. Phys. B 442 (1995) 205, arXiv:hep-ph/9402340.
- [45] D. Becirevic, A.L. Yaouanc, A. Oyanguren, P. Roudeau, F. Sanfilippo, Insight into $D/B \rightarrow \pi \ell \nu_\ell$ decay using the pole models, arXiv:1407.1019.